



Journal Name

COMMUNICATION

## Elucidating the Surface Characteristics and Electrochemistry of High-performance LiNiO<sub>2</sub>

Received 00th January 20xx,  
Accepted 00th January 20xx

Jing Xu<sup>a</sup>, Feng Lin<sup>a</sup>, Dennis Nordlund<sup>b</sup>, Ethan J. Crumlin<sup>c</sup>, Feng Wang<sup>d</sup>, Jianming Bai<sup>e</sup>, Marca M. Doeff<sup>a</sup>, Wei Tong<sup>a</sup>

DOI: 10.1039/x0xx00000x

www.rsc.org/

**Phase pure LiNiO<sub>2</sub> was prepared by a solid-state method and the optimal synthesis condition led to a remarkably high capacity of 200 mAh/g with excellent retention. The combination of bulk and surface characterization elucidated an essential role of the excess Li in phase formation during synthesis and subsequent electrochemical performance.**

At present, Li-ion batteries are considered the most promising energy storage devices for electric vehicles (EVs) and plug-in hybrid electric vehicles (HEVs). However, ultimate goals of high performance and low cost (\$/Wh) need to be achieved in order to replace fuel by electrical power, and realize mass adoption of EVs and HEVs. LiNiO<sub>2</sub> attracted immediate attention in the initial search for alternatives to LiCoO<sub>2</sub> because of the isostructural characteristics and lower cost.<sup>1</sup> Moreover, the electronic configuration of Ni<sup>3+</sup> (3d<sup>7</sup>) in LiNiO<sub>2</sub> allows the removal of electrons only from the e<sub>g</sub> band, so that loss of oxygen occurs at a lower Li content (x in Li<sub>x</sub>MO<sub>2</sub> where M = Co or Ni); i.e., at a higher charge state compared to LiCoO<sub>2</sub>, which translates into higher practical capacity.<sup>2</sup> However, because of the higher Ni content, a severe capacity fade may occur upon cycling, due to the impacts of both structural transformation and surface instability.<sup>3-6</sup> A combination of different transition metals (e.g., LiNi<sub>x</sub>Mn<sub>y</sub>Co<sub>z</sub>O<sub>2</sub> or NMCs) further increases the complexity of the problem since phase separation and side reactions with electrolyte have been reported for different compositions.<sup>7, 8</sup> Therefore, the elucidation of the structural characteristics and their relationship with the electrochemical behavior for pure LiNiO<sub>2</sub>

not only provides insights into synthesizing better performing LiNiO<sub>2</sub> compound but also complement the mechanistic understanding for more complex R-3m layered compounds, such as nickel-rich NMC materials, by isolating synergetic effects from different transition metals.

Stoichiometric LiNiO<sub>2</sub> is challenging to synthesize, due to the tendency for lithium loss and migration of Ni to the lithium layers to form off-stoichiometric Li<sub>1-x</sub>Ni<sub>1+x</sub>O<sub>2</sub>. The presence of excess Ni ions on the Li sites blocks the Li diffusion pathways and imposes a detrimental effect on the electrochemical performance.<sup>9-11</sup> Various conditions that are related to the synthetic routes have been explored and several key variables have been identified. For example, Ohzuku et al. investigated the effects of Li, Ni precursors, and annealing atmosphere on the synthesis of LiNiO<sub>2</sub> by solid state reaction and observed a pronounced effect of the O<sub>2</sub> atmosphere on the stoichiometry and cation arrangement.<sup>12</sup> Reacting LiNO<sub>3</sub> with Ni(OH)<sub>2</sub> or NiCO<sub>3</sub> at 750 °C under O<sub>2</sub> atmosphere produced a product with an initial charge capacity of 180 mAh/g and a reversible discharge capacity of above 150 mAh/g in the voltage range of 2.5 to 4.2 V (0.17 mA/cm<sup>2</sup>). Lu et al. further pointed out that high O<sub>2</sub> partial pressure was necessary to overcome the diffusion barrier existing in the precursor powder.<sup>13</sup> When annealed at a high O<sub>2</sub> flow rate (800 mL/min), the LiNiO<sub>2</sub> product delivered a discharge capacity of > 160 mAh/g with 150 mAh/g remained after 30 cycles (3.0 - 4.3 V, 0.4 mA/cm<sup>2</sup>).<sup>14</sup> In addition, the Li content in the precursor also played a key role in the stoichiometry of the final product. Arai et al. reported the synthesis of a highly stoichiometric LiNiO<sub>2</sub> obtained by mixing an aqueous solution of LiOH·H<sub>2</sub>O and Ni(NO<sub>3</sub>)<sub>2</sub>·6H<sub>2</sub>O with a molar ratio of 4:1 and washing away the large amount of excess Li after calcination. This material delivered a reversible capacity of about 200 mAh/g during 10 cycles (3.0 - 4.5 V, 0.5 mA/cm<sup>2</sup>).<sup>15</sup> These results suggest that the design of LiNiO<sub>2</sub> cathodes could benefit from a systematic study of the relationship between synthesis parameters, structural and chemical characteristics, and electrochemical behaviour. The need for this is reinforced by the fact that different results are obtained when nominally identical

<sup>a</sup> Energy Storage and Distributed Resources Division, Lawrence Berkeley National Laboratory, Berkeley, CA 94720, USA Address here.

<sup>b</sup> Stanford Synchrotron Radiation Lightsource, SLAC National Accelerator Laboratory, Menlo Park, CA 94025, USA

<sup>c</sup> Advanced Light Source, Lawrence Berkeley National Laboratory, Berkeley, California 94720, USA

<sup>d</sup> Department of Sustainable Energy Technologies, Brookhaven National Laboratory, Upton, New York 11973, USA

<sup>e</sup> National Synchrotron Light Source II, Brookhaven National Laboratory, Upton, NY 11973, USA

†Electronic Supplementary Information (ESI) available: See DOI: 10.1039/x0xx00000x

synthesis methods are used by different groups, owing to the complexity of controlling the  $\text{LiNiO}_2$  stoichiometry.<sup>16,17</sup>

Herein, we report a comprehensive study on the effect of various solid-state synthesis parameters on the crystal structures, morphologies, and surface characteristics of layered lithium nickel oxides and correlate these characteristics with electrochemical performance. The best  $\text{LiNiO}_2$  demonstrated excellent electrochemical performance including high discharge capacity, good rate capability, and capacity retention. The work provides insights into the surface chemistries of  $\text{LiNiO}_2$  materials and sheds lights on the design of Ni-based cathode materials for Li-ion batteries.

$\text{LiNiO}_2$  samples were prepared by a solid state method using both commercial and precipitated  $\text{Ni(OH)}_2$  precursors. The synthesis of  $\text{LiNiO}_2$  with the precipitated nickel hydroxide precursor followed the protocol originally designed for lithium nickel manganese cobalt oxide.<sup>4,18</sup> For this, 2% and 10% excess  $\text{LiOH}$  precursors were used, the as-prepared samples are denoted as “solution\_2exLi” and “solution\_10exLi”, respectively. The third sample was simply synthesized following a general solid state reaction protocol by milling  $\text{Li}_2\text{CO}_3$  and  $\text{Ni(OH)}_2$  (Sigma Aldrich) precursors with 10% excess Li, henceforth, referred to as “solid\_10exLi” (for experimental details, see ESI). Figure 1 (a) shows the synchrotron X-ray diffraction (SXRD) patterns of the as-synthesized  $\text{LiNiO}_2$  powders. The high intensity ratios between (003)/(104) and clear peak splits between (108) and (110) suggest good phase crystallinity and cation ordering,<sup>12</sup> which is further confirmed by the Rietveld refinement results (Table S1). Overall, the occupancies of  $3a$  sites by Ni ions are less than 2% for all three samples. Scanning electron microscopy (SEM) images (Figure 1 (b) - (d)) illustrate that the secondary particle size of the as-synthesized powders averages about a few microns and a relatively uniform particle size distribution was observed for the solid\_10exLi sample.

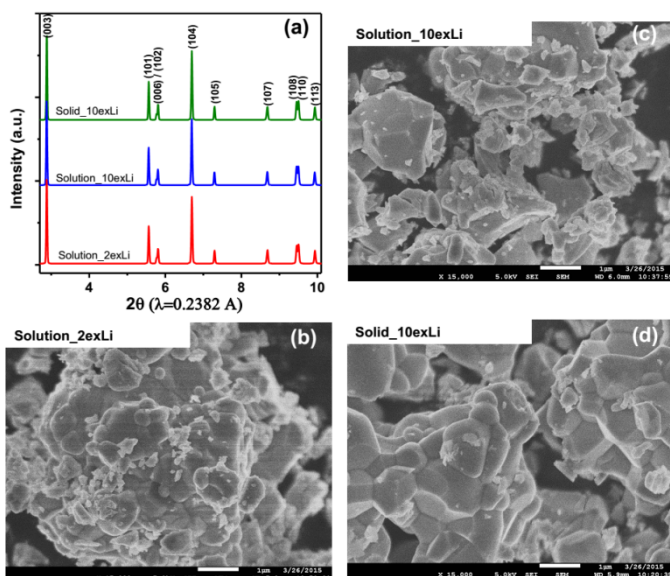


**Figure 1** (a) Synchrotron X-ray diffraction patterns of  $\text{LiNiO}_2$  prepared from solution\_2exLi, solution\_10exLi, and solid\_10exLi. (b), (c) & (d) are SEM images of the as-prepared powders, respectively.

The materials were cycled between 4.3 and 2.7 V at C/10 for the electrochemical tests. The 1<sup>st</sup> cycle voltage profiles are shown in Figure 2 (a). Solution\_2exLi delivered a capacity of 223 mAh/g in the first charge, and 190 mAh/g in the first discharge. The 1<sup>st</sup> cycle electrochemical behaviors of  $\text{LiNiO}_2$  prepared with 10% excess Li (solution\_10exLi and solid\_10exLi) were quite similar, suggesting negligible effect of  $\text{Ni(OH)}_2$  precursor. These two samples delivered a charge capacity of 240 mAh/g (corresponding to 0.85 Li deintercalation) and a discharge capacity of 206 mAh/g (corresponding to 0.73 Li reintercalation). These differences among the samples were repeatable and beyond what would be expected from cell-to-cell variation (< 5 mAh/g) within our experiments, and thus can be considered to result from changing the active material. The higher capacity and lower polarization for these two samples compared to those of solution\_2exLi indicated that the amount of excess Li in the synthesis had a much larger effect on the electrochemical properties than the source of the Ni precursor. Not only did the larger excess of Li have positive effects on the 1<sup>st</sup> cycle capacities, but also better rate capability and capacity retention in the subsequent cycles were observed (Figure 2 (b) and inset). After 20 cycles, 88% discharge capacity was maintained, and the retention was still as high as 75% after 50 cycles. Such good performance has rarely been observed for  $\text{LiNiO}_2$  materials when cycled under similar conditions. In addition, both samples with 10% excess Li exhibited a good rate capability with about 90% capacity retained at 1C. When the current density was further increased, the solid\_10exLi sample delivered a slightly higher capacity than the solution\_10exLi at 2C. This is presumably due to its more uniform particle size distribution as shown by the SEM studies. In contrast, the solution\_2exLi showed slightly lower discharge capacity upon cycling and in the rate test as well. Given that SXRD showed similar lattice parameters and cation ordering for these three samples (Table S1), such differences observed in the electrochemical performance of the samples synthesized with different amounts of excess Li and different types of  $\text{Ni(OH)}_2$  precursor must originate from the surface characteristics. To understand these further, surface-sensitive soft X-ray Absorption Spectroscopy (XAS) and X-ray Photo-electron Spectroscopy (XPS) techniques were employed.

The Ni L3-edge soft XAS spectra of the three pristine

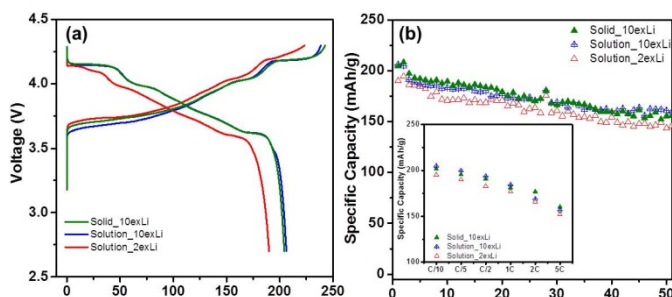


**Figure 2** (a) The 1<sup>st</sup> cycle voltage profiles, (b) cycling performances, and inset rate capabilities of solution\_2exLi, solution\_10exLi, and solid\_10exLi. Cells were cycled between 4.3 and 2.7 V at C/10, capacity at 1C was defined as 180 mAh/g.

powders are shown in Figure 3. In order to avoid contamination from the adhesive on the carbon tape, all the powders were pressed onto Au foil for characterization. Three detection modes, Auger electron yield (AEY), Total electron yield (TEY), and Fluorescence yield (FY), were collected simultaneously. Due to the different mean free paths of electrons and fluorescence in the samples, AEY, TEY and FY modes typically probe 1 - 2 nm, 2 - 5 nm, and  $\sim 50$  nm from the sample surface towards the bulk, respectively.<sup>4</sup> In other words, the information obtained by the soft XAS experiment on the as-prepared samples, which have a particle size of about a few microns, concerns both the surface characteristics (AEY, TEY) and the bulk (FY) of the LiNiO<sub>2</sub> materials. For LiNiO<sub>2</sub>, the most salient electronic structure can be qualitatively obtained through the deconvolution of the Ni L3-edge into high-energy (L3<sub>high</sub>) and low-energy (L3<sub>low</sub>) features. The ratio between L3<sub>high</sub> and L3<sub>low</sub> is in a positive relationship with Ni oxidation state. The three modes (AEY, TEY, and FY) of Ni L3-edge for each sample shown in Figure 3 (a) are normalized with respect to the L3<sub>low</sub> feature. It can be clearly seen that the variation in the Ni oxidation state follows a similar trend from the very surface to the sub-surface for all three of the samples. As evidenced by the increased L3<sub>high</sub>/L3<sub>low</sub> ratios from AEY to FY mode, Ni is more oxidized in the sub-surface region of the LiNiO<sub>2</sub> samples compared to their surfaces; in other words, there is an oxidation state gradient. When comparing each mode across the three samples (Figure 3 (b)), it can be seen

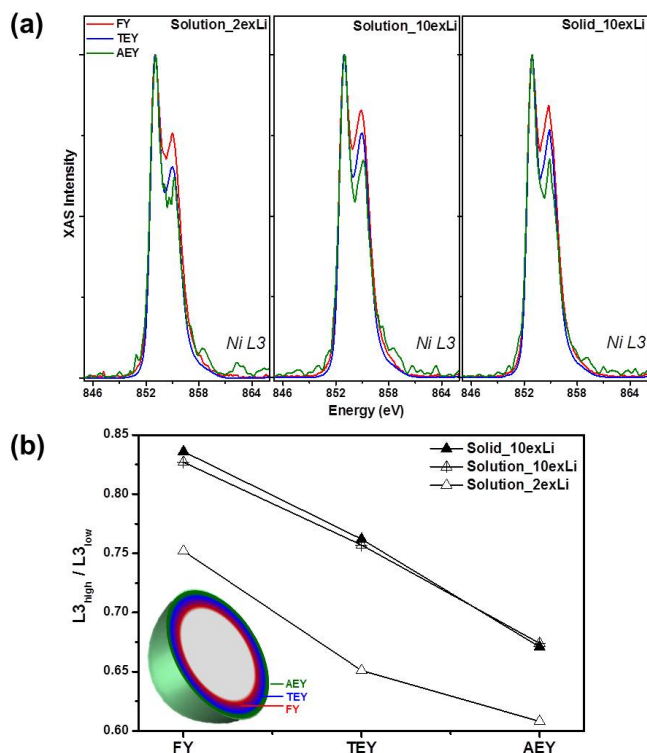


**Figure 3** Soft XAS spectra for the three pristine LiNiO<sub>2</sub> samples. (a) Ni L3-edge spectra from three detection modes with different probing depths (AEY: 1 - 2 nm; TEY: 2 - 5 nm; FY:  $\sim 50$  nm). Note: all the spectra are normalized with respect to the low energy Ni L3-edge, denoted as L3<sub>low</sub>. (b) L3<sub>high</sub>/L3<sub>low</sub> ratios of all three samples at different modes shown in (a).

that the solution\_2exLi has the lowest Ni oxidation state in all three modes, while the L3<sub>high</sub>/L3<sub>low</sub> ratios for the other two samples with 10 % excess Li are very close to each other, indicating similar Ni oxidation states and gradients.

In addition to the study on Ni oxidation state by soft XAS, XPS was also employed to further investigate the surface properties. As can be seen in Figure 4 (a), the main feature of the O1s XPS regions for all three samples is one strong peak around 531.5 eV, which is associated with Li<sub>2</sub>CO<sub>3</sub> on the surfaces.<sup>19, 20</sup> The presence of surface Li<sub>2</sub>CO<sub>3</sub> is also supported by the following observations: (1) the Li1s peak located at 55.5 eV in Figure 4 (b), (2) the C1s peak around 290 eV in the XPS (Figure S1).<sup>19, 20</sup> Close examination of the XPS spectra shows the presence of a small peak with very low intensity at 529.5 eV in the solution\_2exLi and solid\_10exLi samples (Figure 4 (a)) which can be ascribed to O in oxide, in this case the lattice of the active material.<sup>19, 20</sup> The low intensity of the oxide peak indicate that the reaction layer at the surface is a few nm (The O1s XPS was recorded at 670eV, resulting in a very surface sensitive mean free path of less than 1nm). The peak is almost invisible in the XPS spectra of solution\_10exLi sample (Figure 4 (a)). In Figure 4 (b), the Li1s and Ni3p XPS region is plotted across the same three samples, and normalized to the Li1s peak intensity. We find a positive correlation between the intensities of O1s peaks corresponding to oxygen in the lattice (529.5 eV) and those due to Ni3p (67.6 eV). The solution\_10exLi sample exhibits the lowest intensity Ni3p peak while the O1s in the lattice is almost invisible (Figure 4 (a)). In addition, despite the cross-section difference between Li1s and Ni3p at 670 eV excitation,<sup>21</sup> we would expect to see the typical peak of Li1s at about 53.6 eV associated with the Li in the lattice;<sup>22</sup> however, it is missing in all of the three samples. This directly suggests that the surface Ni atoms exist in a NiO-type phase instead of in layered LiNiO<sub>2</sub>. In fact, surface NiO-type phase formation in the solution\_2exLi sample is correlated with the lower valance state of Ni observed by the soft SXAS experiments because Ni in NiO phase is expected to be divalent, whereas it is trivalent in pristine LiNiO<sub>2</sub>. The combination of XPS and soft XAS results leads to the conclusion that Li<sub>2</sub>CO<sub>3</sub> seems to inevitably form on the surface of LiNiO<sub>2</sub> even when the amount of excess lithium-containing precursor is small (2%). The lower amount of lithium-excess

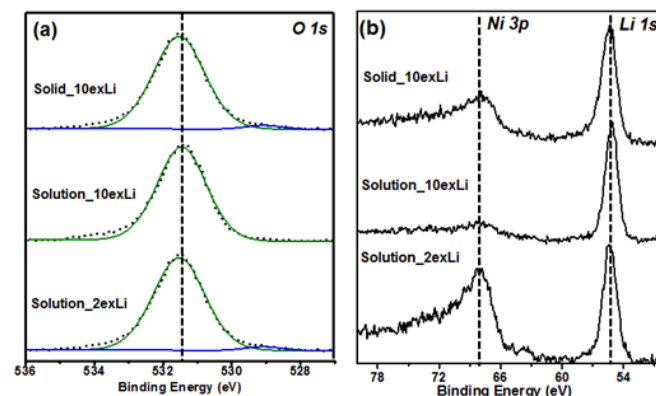


**Figure 4** XPS (a) O1s regions and (b) Ni3p / Li1s regions for pristine solution\_2exLi, solution\_10exLi, and solid\_10exLi, respectively. Dash and solid lines in (a) indicate observed and fitted profiles.

also results in a stronger tendency to form reduced Ni on particle surfaces, probably in the form of a rock salt phase related to NiO. The main role of a sufficiently large Li-excess during solid-state synthesis appears to be in the suppression of NiO-type phase formation containing divalent nickel on particle surfaces, which can impede lithium diffusion during cycling, resulting in inferior electrochemical behavior. The effects of the amount of lithium excess during LiNiO<sub>2</sub> synthesis are subtle, affecting primarily the particle surfaces rather than the bulk, which can explain previous results in samples that appear to have similar bulk properties perform differently.

In summary, stoichiometric LiNiO<sub>2</sub> with excellent electrochemical performance was successfully synthesized by a solid-state method. The synchrotron XRD results proved that all of the as-prepared LiNiO<sub>2</sub> bulk samples were highly crystalline and phase-pure with few defects (< 2% Ni in 3a sites) no matter how much excess lithium was used or what the source of the Ni(OH)<sub>2</sub> starting materials were. However, soft XAS showed that, while Ni tended to be more reduced on the surfaces of all the samples, those made with a higher amount of excess Li (10%) were less extreme in this regard compared to a sample made with only a 2% excess. This information, in combination with the Li1s, Ni3p, and O1s XPS spectra, can be interpreted to mean that Ni on the surface exists in the form of a NiO-type phase, particularly for the sample made with only a 2% excess of lithium. The XPS O1s and C1s spectra also revealed that Li<sub>2</sub>CO<sub>3</sub> preferably formed on the surface of the particles during synthesis even for samples made with a low amount of excess lithium. Both XPS and soft XAS results confirmed the possible formation of NiO-type phase on the surface, which is inversely correlated to the amount of surface Li<sub>2</sub>CO<sub>3</sub> formation. The results indicate that the amount of NiO on the surface can be reduced (although not eliminated entirely) by using a sufficient excess of Li in the synthesis. This study shows a direct correlation between the surface characteristics and superior electrochemical performance, both of which are largely influenced by the amount of excess Li used in the synthesis and explains why samples with similar bulk properties perform differently. This may also have implications for the syntheses and optimization of other Ni-rich layered oxide cathode materials (e.g., LiNi<sub>x</sub>Co<sub>y</sub>Al<sub>1-x-y</sub>O<sub>2</sub> and LiNi<sub>x</sub>Mn<sub>y</sub>Co<sub>1-x-y</sub>O<sub>2</sub> (0 < x, y < 1)) of interest for battery applications.

This work was supported by the Assistant Secretary for Energy Efficiency and Renewable Energy, Office of Vehicle Technologies of the U.S. Department of Energy (DOE) under Contract No. DE-AC02-05CH11231. Soft XAS experiments were carried out at the Stanford Synchrotron Radiation Lightsource, a Directorate of SLAC National Accelerator Laboratory and an Office of Science User Facility operated for the U.S. DOE Office of Science by Stanford University. Use of the Stanford Synchrotron Radiation Lightsource, SLAC National Accelerator Laboratory, is supported by the U.S. DOE, Office of Science, Office of Basic Energy Sciences under Contract No. DE-AC02-76SF00515. J. Bai and F. Wang thank the support by the U.S. DOE Office of Energy Efficiency and Renewable Energy under the Advanced Battery Materials Research (BMR) program,

Contract No. DE-SC0012704. Use of the National Synchrotron Light Source II, Brookhaven National Laboratory, was supported by the U.S. DOE, Office of Science, Office of Basic Energy Sciences, under Contract No. DE-SC0012704. Synchrotron XPS was carried out at beamline 9.3.2 at the Advanced Light Source in Lawrence Berkeley National Laboratory, which is supported by the Director Office of Science, Office of Basic Energy Sciences, of the U.S. DOE under Contract No. DE-AC02-05CH11231.

## References

1. A. Kraysberg and Y. Ein-Eli, *Advanced Energy Materials*, 2012, **2**, 922-939.
2. R. V. Chebiam, F. Prado and A. Manthiram, *Chemistry of Materials*, 2001, **13**, 2951-2957.
3. F. Lin, D. Nordlund, I. M. Markus, T.-C. Weng, H. L. Xin and M. M. Doeff, *Energy & Environmental Science*, 2014, **7**, 3077-3085.
4. F. Lin, I. M. Markus, D. Nordlund, T.-C. Weng, M. D. Asta, H. L. Xin and M. M. Doeff, *Nature Communications*, 2014, **5**.
5. H.-J. Noh, S. Yoon, C. S. Yoon and Y.-K. Sun, *Journal of Power Sources*, 2013, **233**, 121-130.
6. Y.-K. Sun, D.-J. Lee, Y. J. Lee, Z. Chen and S.-T. Myung, *ACS Applied Materials & Interfaces*, 2013, **5**, 11434-11440.
7. J. M. Zheng, W. H. Kan and A. Manthiram, *Acs Applied Materials & Interfaces*, 2015, **7**, 6926-6934.
8. P. F. Yan, J. M. Zheng, D. P. Lv, Y. Wei, J. X. Zheng, Z. G. Wang, S. Kuppen, J. G. Yu, L. L. Luo, D. Edwards, M. Olszta, K. Amine, J. Liu, J. Xiao, F. Pan, G. Y. Chen, J. G. Zhang and C. M. Wang, *Chemistry of Materials*, 2015, **27**, 5393-5401.
9. B. L. Ellis, K. T. Lee and L. F. Nazar, *Chemistry of Materials*, 2010, **22**, 691-714.
10. C. Li, H. P. Zhang, L. J. Fu, H. Liu, Y. P. Wu, E. Ram, R. Holze and H. Q. Wu, *Electrochimica Acta*, 2006, **51**, 3872-3883.
11. A. Rougier, P. Gravereau and C. Delmas, *Journal of the Electrochemical Society*, 1996, **143**, 1168-1175.
12. T. Ohzuku, A. Ueda and M. Nagayama, *Journal of the Electrochemical Society*, 1993, **140**, 1862-1870.
13. C. H. Lu and L. Wei-Cheng, *Journal of Materials Chemistry*, 2000, **10**, 1403-1407.
14. K. S. Park, S. H. Park, Y. K. Sun, K. S. Nahm, Y. S. Lee and M. Yoshio, *Journal of Applied Electrochemistry*, 2002, **32**, 1229-1233.
15. H. Arai, S. Okada, H. Ohtsuka, M. Ichimura and J. Yamaki, *Solid State Ionics*, 1995, **80**, 261-269.
16. T. Ohzuku, A. Ueda and M. Nagayama, *Journal of The Electrochemical Society*, 1993, **140**, 1862-1870.
17. A. Rougier, P. Gravereau and C. Delmas, *Journal of The Electrochemical Society*, 1996, **143**, 1168-1175.
18. F. Lin, D. Nordlund, T. Pan, I. M. Markus, T.-C. Weng, H. L. Xin and M. M. Doeff, *Journal of Materials Chemistry A*, 2014, **2**, 19833-19840.
19. A. M. Andersson, D. P. Abraham, R. Haasch, S. MacLaren, J. Liu and K. Amine, *Journal of the Electrochemical Society*, 2002, **149**, A1358-A1369.
20. N. Yabuuchi, K. Yoshii, S. T. Myung, I. Nakai and S. Komaba, *Journal of the American Chemical Society*, 2011, **133**, 4404-4419.
21. J. J. Yeh and I. Lindau, *Atomic Data and Nuclear Data Tables*, 1985, **32**, 1-155.
22. M. Oku, H. Tokuda and K. Hirokawa, *Journal of Electron Spectroscopy and Related Phenomena*, 1991, **53**, 201-211.